Quantum networking with single ions

Jürgen Eschner

Universität des Saarlandes, Experimentalphysik
Campus E2 6, 66123 Saarbrücken, Germany

Summary. — This lecture addresses the application of trapped single ions in the context of quantum networks. It intends to provide an introduction into the basic physical principles, the experimental challenges, and the state of the art.

1. – Motivation

Since their first experimental preparation [1], single trapped ions have consistently defined the state-of-the-art in the control of atom-photon interaction at the level of single quantum systems. After early demonstrations of fundamental quantum effects such as, e.g., anti-bunching [2] and quantum jumps [3, 4, 5], they have more recently been the platform with which the first [6, 7, 8] and the most advanced [9] quantum information processing tasks have been implemented. They have also provided, as of now, the highest degree of sophistication in multi-qubit quantum simulations [10, 11].

Single photons, on the other hand, have been used to demonstrate quantum non-locality [12], the violation of Bell inequalities [13], and multi-qubit entanglement [14]. Photon pairs from parametric down-conversion [15] are a convenient resource of high-purity entanglement. Together with their easy manipulation and transmission, this makes photons the natural platform for quantum communication tasks such as, e.g., quantum cryptography [16].

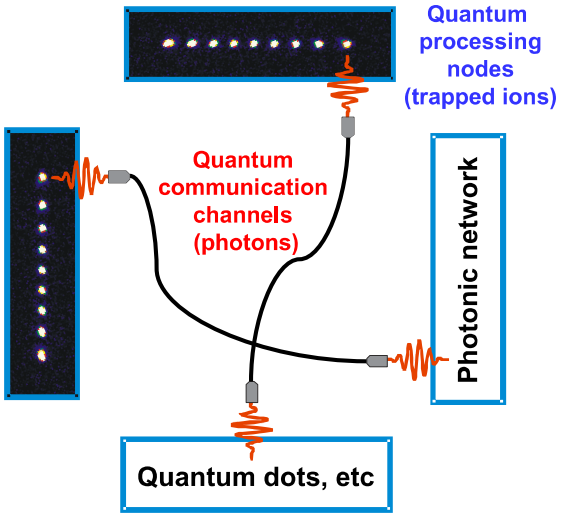

Fig. 1. – A quantum network. At the nodes, atomic quantum systems such as single ions or quantum dots store and process quantum information. Photonic channels connect the nodes and transmit the information. At the interfaces, quantum information is converted between atomic and photonic quantum bits. Photonic networks may also be integrated.

A quantum network [17], as schematically depicted in Fig. 1, is a comprehensive vision that integrates local processing of quantum information with its communication over macroscopic distances. In this context, single ions (or chains of ions) are natural and promising implementations of stationary qubits on which computations are carried out, while single photons serve as quantum channels that transfer quantum information and mediate entanglement between the atomic network nodes [18]. Such nodes are, of course, not restricted to trapped ions or atoms but may also be implemented employing other atom-like media, such as single quantum excitations in solid state systems or superconducting circuits.

Basic considerations will be discussed in section **2**, while in section **3** the experimental state-of-the-art will be reviewed. The final section **4** gives a brief summary and outlook.

2. – Basic considerations and principles

The main experimental challenge in the construction of a quantum network, in addition to the ongoing efforts in processing and transmitting quantum information, is the controlled conversion of quantum information between atoms and photons, the atom-photon interface. Faithful conversion is the prerequisite for quantum coherence throughout the network, in particular for establishing entanglement between the nodes via the channels. Figure 2 illustrates some procedures which have been proposed for establishing such entanglement. Direct photonic interaction [19] reads out a quantum state from a

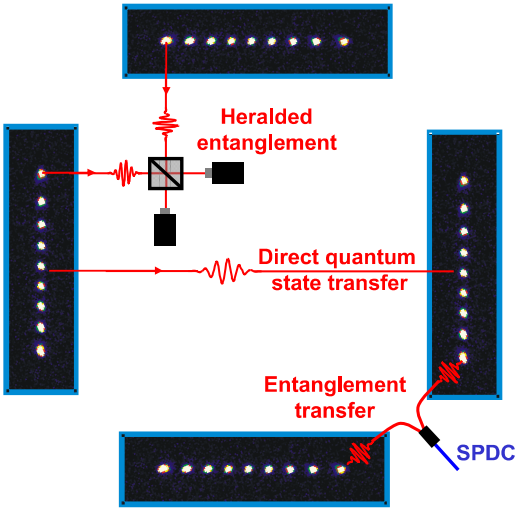

Fig. 2. – Schemes for creating distant atomic entanglement. SPDC stands for a source of entangled photon pairs based on spontaneous parametric down-conversion. See text for more details.

stationary qubit in one node and transmits it to another node where it is written into another qubit. Heralded entanglement [20, 21, 22] is created through an entanglement-swapping procedure, starting from simultaneous atom-photon entanglement at two nodes, followed by photon detection. Entanglement transfer [23] uses photon pairs as a resource for entanglement, and transfers it into a pair of distant atoms. These methods will be discussed in more detail below.

2˙1. *Atom-photon entanglement.* – The most important fundamental principle from which all such schemes benefit is atom-photon entanglement: when an atom, prepared in a well-defined initial state, emits a photon on one of several possible transitions, then the final state of the atom will be quantum-correlated with the state of this photon. This is illustrated in Fig. 3. In this generic example, an atom decays from an upper state $|m'\rangle$ to several possible lower states $|m = m'\rangle$, $|m-1\rangle$, or $|m+1\rangle$ via emission of a correspondingly π-, σ^+-, or σ^--polarized photon. The combined atom-photon state after emission is entangled according to

$$|\psi\rangle_{\mathrm{atom-photon}} = g_0|m\rangle|\pi\rangle + g_-|m-1\rangle|\sigma^+\rangle + g_+|m+1\rangle|\sigma^-\rangle \tag{1}$$

whereby the coefficients $g_{0,-,+}$ are determined by the Clebsch-Gordan coefficients of the transitions, by the geometry used in a specific experimental setting, and, possibly, by optical propagation phases.

The quantum correlation may comprise all physical properties of the photon: polarization, frequency, phase, direction. This implies that in order to generate qubit

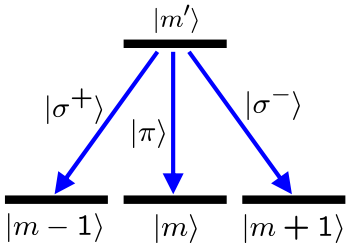

Fig. 3. – Generic scheme for atom-photon entanglement. The final atomic state after emission of a photon is entangled with the properties (here with the polarization) of the emitted photon. m, m' are magnetic quantum numbers, $\pi, \sigma^{\pm}$ are photon polarizations.

entanglement, i.e., of two spin-$\frac{1}{2}$-like degrees of freedom, a selection (or projection) may have to be applied. As an example, Fig. 4 illustrates the selection of a certain direction of propagation of the photon.

If the atomic Zeeman sublevels are non-degenerate with an energy splitting of $\hbar\Delta$, as shown in the example of Fig. 5, photons emitted with different polarizations will have different frequencies, corresponding to a Larmor precession in the atom at frequency Δ, which leads to an additional phase $\mathrm{e}^{\mathrm{i}\Delta t}$ in the entangled state:

$$|\psi\rangle_{\mathrm{atom-photon}} = g_-|-1\rangle|\sigma^+\rangle + g_+\mathrm{e}^{\mathrm{i}\Delta t}|+1\rangle|\sigma^-\rangle \tag{2}$$

Having this frequency information available (for example by using a narrow-bandwidth optical filter) would destroy the entanglement of the polarization with the atomic state. The information may, however, be erased by measuring the arrival time of the photon with temporal resolution much better than the Larmor precession period [24].

Starting from an atom which is prepared in a single sublevel of its ground state, a

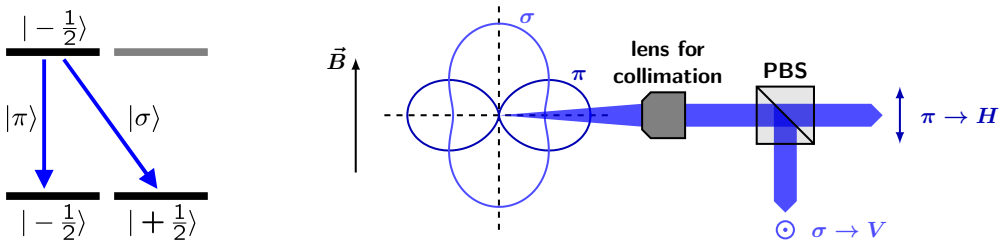

Fig. 4. – Example for qubit-type atom-photon entanglement (after [25]). Left: An $|m' = -\frac{1}{2}\rangle$ Zeeman sublevel from a $J' = \frac{1}{2}$ manifold decays into either $|m = -\frac{1}{2}\rangle$ or $|m = +\frac{1}{2}\rangle$ of another $J = \frac{1}{2}$ manifold. Right: Photons emitted on the π- or σ-transition (i.e. $\Delta m = 0$ or ± 1, respectively) and emitted at 90° to the quantization axis are linearly polarized along the magnetic field direction ($\pi \rightarrow H$) or orthogonal to it ($\sigma \rightarrow V$). The atomic qubit $|m = \pm\frac{1}{2}\rangle$ will be entangled with the photonic polarization qubit $|H, V\rangle$. PBS stands for polarizing beam splitter.

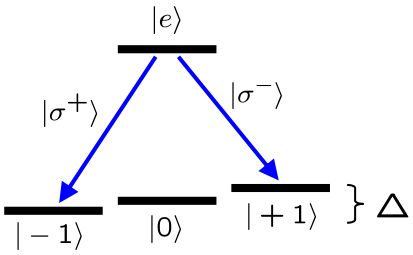

Fig. 5. – Atom-photon entanglement with non-degenerate atomic Zeeman sublevels. Due to the energy splitting by $\hbar\Delta$, the entangled state has an additional time-dependent phase $e^{i\Delta t}$, see text.

"poor man's" version of generating atom-photon entanglement may be implemented, as displayed in Fig. 6: by weakly exciting an atom that is initially in one sublevel of its ground state, a Raman transition to another sublevel is induced with small probability ϵ. The photonic degree of freedom is the number of emitted photons, 0 or 1. In the example, the entangled state is

$$|\psi\rangle_{\mathrm{atom-photon}} = \epsilon^{1/2}|+\frac{1}{2}\rangle|1\rangle_\sigma + (1-\epsilon)^{1/2}|-\frac{1}{2}\rangle|0\rangle_\sigma \tag{3}$$

This procedure is the basis for one method of creating distant atom-atom entanglement, as will be explained in the following subsection.

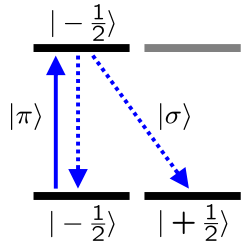

Fig. 6. – Scheme for "poor man's" atom-photon entanglement based on Raman scattering with small probability. The atom is initially in the $-\frac{1}{2}$ sublevel of the ground state and excited with π-polarized light, such that a σ-polarized photon may be released.

2˙2. *Atom-atom entanglement.* – Starting from atom-photon entanglement, two distant atoms may be entangled. The first scheme, proposed by Cabrillo et al. [20] and illustrated in Fig. 7, relies on the "poor man's" entanglement just explained: two distant atoms are prepared in the initial state $|\Psi\rangle_{\mathrm{atom-atom}} = |0\rangle_1|0\rangle_2$ (using the state labeling in the figure), and a Raman scattering process with small transition probability is driven in both atoms simultaneously. Emission from the two atoms is imaged onto a detector

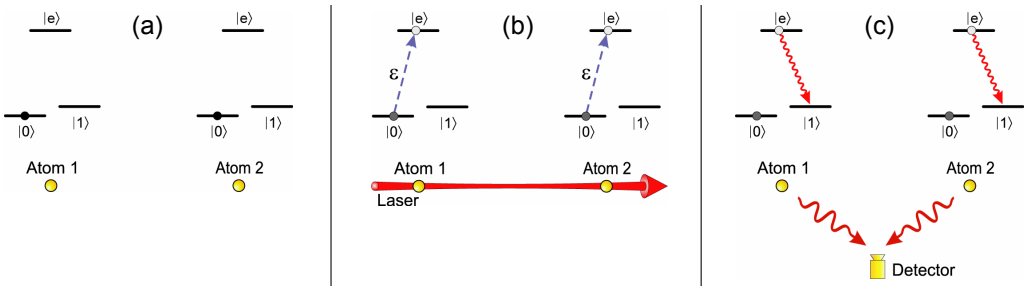

Fig. 7. – Atom-atom entanglement based on small-probability Raman scattering [20]. (a) Both atoms are prepared in the same initial state $|0\rangle$. (b) They are simultaneously excited to an excited state $|e\rangle$ with probability $\epsilon \ll 1$; the exciting light fields at the positions of the two atoms are phase-coherent. (c) If a photon corresponding to the $|e\rangle \to |1\rangle$ transition is detected and the two emission paths are indistinguishable, the quantum state of the combined system is projected into a maximally entangled state, Eq. (4).

somewhere between them in such a way that the two emission paths are indistinguishable (typically by superimposing them on a beam splitter). Neglecting the small (ϵ^2) probability that two photons may have been emitted, the detection of one scattered photon projects the atoms into the maximally entangled state

$$|\Psi\rangle_{\mathrm{atom-atom}} = \frac{1}{\sqrt{2}}\left(|1\rangle_1|0\rangle_2 + \mathrm{e}^{\mathrm{i}\phi}|0\rangle_1|1\rangle_2\right) \tag{4}$$

The phase $\mathrm{e}^{\mathrm{i}\phi}$ in the final state corresponds to the classical interferometer phase between the first beam splitter, where the two excitation beams are created, and the final beam splitter where the two scattering paths are combined in front of the detector. This implies that the set-up has to be interferometrically stable in order to reliably create the entangled two-atom state.

Another scheme, proposed some time later [21], relies on the atom-photon entanglement procedure shown in Fig. 4 and on Hong-Ou-Mandel interference or photon coalescence. The latter denotes the fact that two identical photons that enter simultaneously the two input ports of a beam splitter will leave at the same output port [26]. Figure 8 illustrates how this is utilized for the creation of atom-atom entanglement: both atoms are initially prepared in the same excited state $|e\rangle$. When they decay to either $|0\rangle$ or $|1\rangle$, they will release correspondingly H- or V-polarized photons. This leaves the whole system in the product state $|\Psi\rangle = (g_0|0\rangle|H\rangle + g_1|1\rangle|V\rangle)_1 \times (g_0|0\rangle|H\rangle + g_1|1\rangle|V\rangle)_2$. The emission paths are superimposed on a beam splitter, such that if two photons of the same polarization are emitted, they will coalesce due to Hong-Ou-Mandel interference. Therefore, if two photons are simultaneously recorded on the detectors behind the beam splitter, they must have different polarizations, and the quantum state of the combined

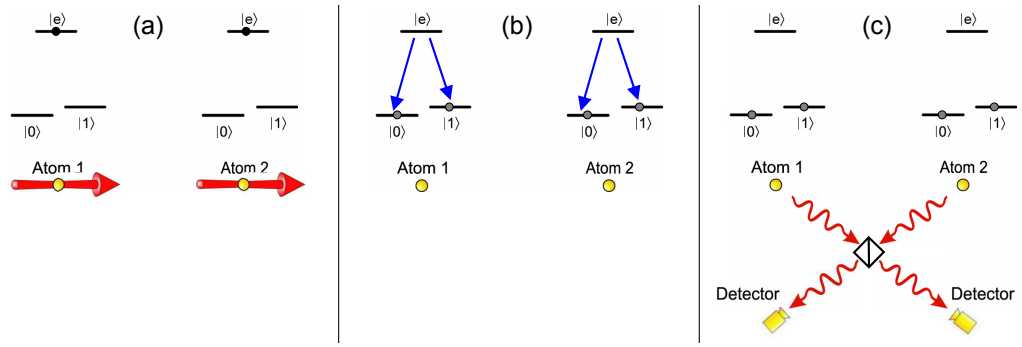

Fig. 8. – Atom-atom entanglement based on Hong-Ou-Mandel interference [21]. (a) Two atoms are prepared in the same excited state $|e\rangle$. (b) Decay to either $|0\rangle$ or $|1\rangle$ releases correspondingly polarized photons. (c) The emission paths into the detectors are superimposed on a beam splitter. Coincident photon detection on the two detectors heralds the entangled atom-atom state, Eq. (5).

system is projected into a maximally entangled state,

$$|\Psi\rangle_{\mathrm{atom-atom}} = \frac{1}{\sqrt{2}}\left(|0\rangle_1|1\rangle_2 - |1\rangle_1|0\rangle_2\right) \tag{5}$$

2˙3. *Atom-photon interfaces.* – As explained in the previous section, atom-photon entanglement is a necessary ingredient for establishing a quantum link between distant single atoms or ions. From a more general perspective, it is only one aspect of the controlled interaction between single atoms and single photons which quantum networks require. Protocols that allow for such controlled interaction have been termed atom-photon interfaces. They comprise both controlled emission as well as controlled absorption of photons.

2˙3.1. Controlled emission. The properties of single photons which may be tailored in a controlled emission process comprise their temporal and spectral structure, their polarization (including entanglement with the atom), and their geometry or spatial mode. An important concept in this respect is that of a single-mode photon. This may be operationally defined from an experimental point of view: the above properties must be engineered in such a way that two photons of the same kind interfere with full contrast. Regarding spatial properties such as distribution and wavefront, a pragmatic definition is that one can couple the photons into a single-mode fiber. This raises already a fundamental experimental challenge because single-mode coupling (just like photon detection) will always happen with less than unity efficiency; therefore a trade-off arises between the probability to obtain a photon and its single-mode character. This will be discussed in more detail later.

First the spectro-temporal character shall be considered more closely: what is the

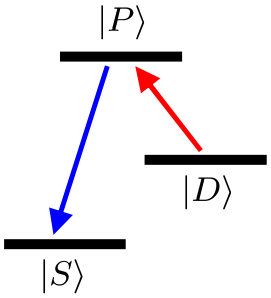

Fig. 9. – Generic scheme for single-photon generation in a 3-level atom. The atom is prepared in a (meta)stable level $|D\rangle$, resonantly excited with a "red" laser to an upper level $|P\rangle$ which decays into a third, stable, level $|S\rangle$ through emission of a single "blue" photon.

wave packet, or envelope function $u_{\rm photon}(t)$, of a single photon, and what is its spectrum? As a first reminder, because we are dealing with a single photon, the spectro-temporal properties (in fact, all properties) are described by distributions that one obtains through repeated measurements. As an example, single photon emission from a single atom may be repeatedly triggered by an exciting laser pulse at time $t = 0$, and a single-photon detector records an arrival time distribution $p_{\rm arrival}(t)$. One may be tempted to say that $p_{\rm arrival}(t) = |u_{\rm photon}(t)|^2$, but the situation is more complex: since the photon may not be fully coherent, the appropriate description of its temporal properties is a coherence function $g^{(1)}_{\rm photon}(t,t') = \langle u^*(t)u(t')\rangle$ (where $\langle\cdot\rangle$ denotes averaging over many individual measurements), and one has $p_{\rm arrival}(t) = g^{(1)}_{\rm photon}(t,t)$ (after proper normalization). Only a spectro-temporally fully coherent photon has a well-defined envelope $u_{\rm photon}(t)$, which one may call a pure state with respect to its spectro-temporal properties ([1]); this shall also be called a Fourier-limited photon. The latter indicates that such a photon will have a spectral width according to the Fourier transform of its temporal shape. This is an important aspect in scenarios where single-photon based quantum communication is combined with frequency multiplexing: Fourier-limited photons allow for the most efficient use of the available bandwidth.

To be more specific, it is useful to consider a generic scheme of single-photon generation from a 3-level atom as displayed in Fig. 9. Assuming no technical noise and a near-unity $|P\rangle \to |S\rangle$ branching ratio (its influence will be examined below), there are two limiting cases: sudden or slow excitation. Sudden coherent $|D\rangle \to |P\rangle$ excitation (i.e., a "red" π-pulse) will put the atom into state $|P\rangle$ with certainty. The resulting "blue" photon will have a temporal distribution corresponding to the natural decay time and a bandwidth corresponding to the linewidth of the $|P\rangle$ state; it will thus be Fourier-

([1]) The functions $u_{\rm photon}(t)$ and $g^{(1)}_{\rm photon}(t,t') = \langle u^*(t)u(t')\rangle$ resemble a pure and mixed quantum state, with time-resolved photon detection constituting a projective measurement, but defining this properly involves some theoretical issues [27], which we did not want to address here.

limited. Slow excitation, on the other hand, drives a spontaneous Raman scattering process: per unit time, a small part of the initial $|D\rangle$ population is transferred to $|P\rangle$ from where it decays to $|S\rangle$. Since this scattering process starts and finishes in levels of well-defined energy, and the laser is assumed monochromatic, the only uncertainty is the duration of the scattering process. Hence the emission time distribution determines also the spectral distribution. Again, also in this case the blue photon will be Fourier-limited. It is important to emphasize that a single photon created by this kind of slow Raman scattering may have a spectral bandwidth much narrower than the linewidth of the upper atomic level!

Possible causes of decoherence in this process of generating a pure single-photon quantum state include both technical deficiencies and fundamental issues. On the technical side, any jitter in the emission time or frequency, resulting for example from fluctuations in the laser frequency or intensity or from magnetic field noise, will lead to non-maximal coherence. Even without these, however, an important fundamental limitation is set by the branching ratio of the upper level: in the case of slow Raman excitation, if the atom may decay back on the red $|P\rangle \rightarrow |D\rangle$ transition with some probability before releasing the blue photon, then the emission time distribution of the blue photon suffers a corresponding broadening. In other words, without knowing how many red photons have been scattered before the single blue photon was emitted, one creates a mixed state that averages over all possibilities of previous red photon emission. The mixing will be small or large if the branching ratio favors strongly blue or red emission, respectively [28, 29, 30]. A pure state, or Fourier-limited photon, requires that the probability for $|P\rangle \rightarrow |D\rangle$ decay be very small (or that one keeps track of all previously emitted red photons, which is rather unpractical).

The influence of the branching ratio also illustrates the trade-off between state purity and generation efficiency: taking as an example sudden $|D\rangle \rightarrow |P\rangle$ excitation, the resulting blue photon will be Fourier-limited as explained above. But it will only be created in a fraction of the cases, corresponding to the $|P\rangle \rightarrow |S\rangle$ branching ratio. For slow excitation, one may create the blue photon with certainty by driving the red transition long enough, but a non-unity branching ratio leads to state impurity as explained above. One may think about purifying the blue photon by only using the initial part of its emission time distribution, thereby suppressing cases where intermediate red photons were created, but this again happens at the expense of generation efficiency. Similar considerations hold for the spatial and polarization degrees of freedom.

2˙3.2. Controlled absorption. In controlled absorption, the ultimate goal is to transfer the quantum state of an incoming photon to the absorbing atom with high fidelity and high success probability. This ideal case may be approached via several levels of increasing control. A simple case is that the state of an atom is monitored via fluorescence, and a quantum jump, i.e., a transition from dark to bright (or the inverse) signals absorption of a single photon [3, 4, 31]. While this method allows detecting incoming photons with extremely high sensitivity, it provides little information about the precise instant of the absorption, or about the resulting atomic state. This method could nevertheless be com-

bined with spatial and spectro-temporal mode matching in order to obtain high (up to near-deterministic) absorption probability. Spectro-temporal mode-matching has been discussed theoretically for a long time [32, 33, 34], even controversially. Here it should suffice to note that the conditions are fundamentally different depending on the considered atomic level scheme: in a two-level system, an inverse exponential temporal shape has been shown to be optimal [35], but this does not offer the same advantage when a three-level system is considered. For spatial mode-matching, the relevant considerations are the same as for collecting a single emitted photon into a single mode; hence, one also expects the same efficiency limitations. The factors that enter into the absorption probability are: (i) the effective solid angle from which light is focused onto the ion, or, in more detail, the spatial overlap of the incoming radiation field with the dipole pattern of the radiation corresponding to the transition that one wants to excite; (ii) the oscillator strength of the transition, which in this context is the same as the probability for a perfectly dipole-shaped incoming wave to excite the transition; (iii) possible cavity enhancement of the interaction strength. Approaches that are being pursued include a deep parabolic mirror around a single ion [32], a high-NA Fresnel lens [36] or optical cavities [37] (so far only with neutral atoms). One may also employ optical pumping for polarization control, i.e., in order to select a certain polarization that can be absorbed, while the orthogonal one is rejected [38]. Instead of pursuing near-deterministic absorption, schemes have been devised where the absorption event is heralded by a released photon [39]. This opens up the possibility of high-fidelity photon-to-atom quantum state transfer [23, 40] without depending critically on spatial mode matching (although this will always be advantageous). An example which may be applied to spin-$\frac{1}{2}$ ions (such as Ca^+, Ba^+, and many others) is shown in Fig. 10.

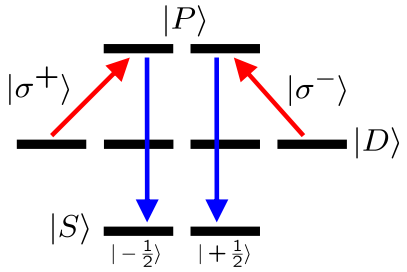

Fig. 10. – Scheme for heralded photon-to-atom quantum state transfer [39, 40, 41] for a spin-$\frac{1}{2}$ atom. The atom is prepared in a superposition of sublevels in the $|D\rangle$ manifold, in which it may absorb an incoming photon of any polarization. By subsequent emission of a π-polarized photon on the $|P\rangle \rightarrow |S\rangle$ transition, the polarization qubit of the absorbed photon is stored in a superposition of the sublevels of $|S\rangle$. Detection of the emitted photon heralds the successful quantum state transfer.

3. – Experiments

3˙1. *Atom-photon and atom-atom entanglement.* – In this section, experiments are summarized that have demonstrated and/or utilized atom-photon and atom-atom entanglement with single ions.

3˙1.1. Atom-photon entanglement.
Atom-photon entanglement has been demonstrated for the first time with a single ion in C. Monroe's group [25], and later with a single trapped neutral atom [42]. Similar results have been reported with cavity-enhanced single-photon emission from a single ion [43] or neutral atom [44]. An early experiment in P. Toschek's group, showing correlations between successively emitted single photons [45], may also be interpreted in terms of atom-photon entanglement.

3˙1.2. Atom-atom entanglement.
Based on these results, atom-atom entanglement has first been demonstrated with two single ions in C. Monroe's group [46], and thereafter with two neutral atoms, employing the scheme of Simon et al. [21]. The scheme of Cabrillo et al. [20] has been experimentally realized more recently [47]. In contrast to the latter work where both entangled ions were stored in the same trap with few μm distance, the former work showed atomic entanglement over macroscopic distances on the meter scale. Employing atom-atom entanglement, quantum state teleportation between distant ions was also realized [48].

For completeness, it may be added that atom-atom entanglement has also been demonstrated in experiments by Haroche's group employing single atoms that interact successively with the field in a high-finesse microwave resonator [49].

3˙2. *Atom-photon interfaces.* – A summary of experiments aiming at the control of single-photon emission and absorption, i.e. towards bi-directional quantum state transfer, is given below.

3˙2.1. Controlled emission.
Controlled single-photon emission from a single ion was first realized in H. Walther's group [50], using a single Ca^+ ion in an optical resonator. The temporal wave packet of the photon was tailored into various shapes, including a double-peaked distribution (similar to a time-bin qubit [51], but its coherence was not investigated). Further developments include the demonstration of high-quality indistinguishability [52], near-Fourier-limited single photons [28], and single photons in a single quantum state at high generation rates [29]. An interesting approach to increase the photon generation rate into a specific spatial mode, beyond what is being pursued with optical resonators [53, 50, 54], is the use of a deep parabolic mirror that converts an outgoing dipole emission pattern into a near-Gaussian beam [34]. The current status is that a single photon is captured with about 81% probability [55]; a new experimental challenge arises through the mirror arrangement, however, because the complex polarization pattern that it produces makes further mode-shaping necessary. Another approach with potentially better scalability

and integration with ion strings in complex trap geometries is the use of Fresnel lenses [36].

A significant amount of work towards controlled single-photon emission has been carried out with single neutral atoms, and single-photon sources based on solid-state emitters are also a very active field; both topics reach beyond what can be addressed in this lecture.

3˙2.2. Controlled absorption.
Absorbing an incoming photon by a single ion with high probability is a formidable experimental challenge. First proof-of-principle experiments have been carried out in our group at Saarland University [56], and previously at ICFO. For that purpose, a photon pair source was constructed that delivers heralded single photons at 854 nm matching in frequency and bandwidth the $D_{5/2}$ to $P_{3/2}$ transition in the $^{40}Ca^{+}$ ion [57, 58]. Interaction between the source photons and a single ion was first observed as an increased depletion rate of the $D_{5/2}$ level [59]. Then the photon pair source was operated as a heralded single photon source, and the temporal and frequency correlation between the herald and the absorption event was demonstrated [60]. In a subsequent experiment, also the polarization correlation was observed, which means that the entanglement between herald and absorbed photon became manifest in the correlation. The maximally entangled state of the photon pair was reconstructed from these correlations by quantum state tomography [38]. As the latest progress towards controlled single-photon absorption, a protocol that heralds the successful absorption event [23, 40] has recently been implemented with a single $^{40}Ca^{+}$ ion, through detection of the single photon that is released by spontaneous Raman scattering after the absorption process. Using this heralding method in combination with coherent preparation of the absorbing ion in a superposition of Zeeman sub-levels, the protocol for high-fidelity photon-to-atom state transfer shown in Fig. 10 has been experimentally demonstrated [39].

4. – Summary and Outlook

The bi-directional atom-photon quantum interface is the central building block for realizing a quantum network with single ions and photons. The experimental progress towards high-fidelity and efficient state transfer in emission and absorption is encouraging. Further milestones shall be reached by combining various methods, such as heralded state transfer with cavity enhancement or with a parabolic mirror. Another important step will be to combine ion-photon interfaces with quantum gates on ion strings, as sketched in Fig. 1. Like for quantum information processing, single ions have proven to be a suitable and promising platform to set the stage for a small-scale quantum network through the development and demonstration of the relevant experimental protocols.

* * *

I would like to thank the directors of the Varenna Summer School on "Applications of Trapped Ions", Martina Knoop, Irene Marzoli, and Giovanna Morigi for the opportunity

to present this lecture and to enjoy the stimulating atmosphere of the school. I would also like to thank Barbara Alzani and the SIF staff at Varenna for their fantastic hospitality, and for making things work. Research at the Universität des Saarlandes has been partially supported by the BMBF ("QuOReP" and "QSCALE" projects), the Krupp-Stiftung, the Alexander von Humboldt Stiftung, and by CONICYT. Pascal Eich's help in the preparation of the manuscript is gratefully acknowledged.

REFERENCES

[1] Neuhauser W., Hohenstatt M., Dehmelt H. and Toschek P. E., *Phys. Rev. A*, **22** (1980) 1137.
[2] Diedrich F. and Walther H., *Phys. Rev. Lett.*, **58** (1987) 203.
[3] Nagourney W., Sandberg J. and Dehmelt H., *Phys. Rev. Lett.*, **56** (1986) 2797.
[4] Sauter T., Neuhauser W., Blatt R. and Toschek P. E., *Phys. Rev. Lett.*, **57** (1986) 1696.
[5] Bergquist J. C., Hulet R., Itano W. M. and Wineland D. J., *Phys. Rev. Lett.*, **57** (1986) 1699.
[6] Monroe C., Meekhof D. M., King B. E., Itano W. M. and Wineland D. J., *Phys. Rev. Lett.*, **75** (1995) 4714.
[7] Schmidt-Kaler F., Häffner H., Riebe M., Gulde S., Lancaster G. P. T., Deuschle T., Becher C., Roos C. F., Eschner J., and Blatt R., *Nature*, **422** (2003) 408.
[8] Leibfried D., DeMarco B., Meyer V., Lucas D., Barrett M., Britton J., Itano W. M., Jelenković B., Langer C., Rosenband T. and Wineland D. J., *Nature*, **422** (2003) 412.
[9] Schindler P., Nigg D., Monz T., Barreiro J. T., Martinez E., Wang S. X., Quint S., Brandl M. F., Nebendahl V., Roos C. F., Chwalla M., Hennrich M. and Blatt R., *New J. Phys.*, **15** (2013) 123012.
[10] Schindler P., Müller M., Nigg D., Barreiro J. T., Martinez E. A., Hennrich M., Monz T., Diehl S., Zoller P. and Blatt R., *Nature Phys.*, **9** (2013) 361.
[11] Islam R., Senko C., Campbell W. C., Korenblit S., Smith J., Lee A., Edwards E. E., Wang C.-C. J., Freericks J. K. and Monroe C., *Science*, **340** (2013) 583.
[12] Pan J.-W., Bouwmeester D., Daniell M., Weinfurter H. and Zeilinger A., *Nature*, **403** (2000) 515.
[13] Aspect A., Dalibard J. and Roger G., *Phys. Rev. Lett.*, **49** (1982) 1804.
[14] Pan J.-W., Chen Z.-B., Lu C.-Y., Weinfurter H., Zeilinger A. and Żukowski M., *Rev. Mod. Phys.*, **84** (2012) 777.
[15] Kwiat P. G., Mattle K., Weinfurter H. and Zeilinger A., *Phys. Rev. Lett.*, **75** (1995) 4337.
[16] Jennewein T., Simon C., Weihs G., Weinfurter H. and Zeilinger A., *Phys. Rev. Lett.*, **84** (2000) 4729.
[17] Kimble H. J., *Nature*, **453** (2008) 1023.
[18] Maunz P., Olmschenk S., Hayes D., Matsukevich D. N., Duan L.-M. and Monroe C., *Phys. Rev. Lett.*, **102** (2009) 250502.
[19] Cirac J. I., Zoller P., Kimble H. J. and Mabuchi H., *Phys. Rev. Lett.*, **78** (1997) 3221.
[20] Cabrillo C., Cirac J. I., García-Fernández P. and Zoller P., *Phys. Rev. A*, **59** (1999) 1025.

[21] Simon C. and Irvine W. T. M., *Phys. Rev. Lett.*, **91** (2003) 110405.
[22] Hofmann J., Krug M., Ortegel N., Gérard L., Weber M., Rosenfeld W. and Weinfurter H., *Science*, **337** (2012) 72.
[23] Lloyd S., Shahriar M. S., Shapiro J. H. and Hemmer P. R., *Phys. Rev. Lett.*, **87** (2001) 167903.
[24] Togan E., Chu Y., Trifonov A. S., Jiang L., Maze J., Childress L., Dutt M. V. G., Sorensen A. S., Hemmer P. R., Zibrov A. S. and Lukin M. D., *Nature*, **466** (2010) 730.
[25] Blinov B. B., Moehring D. L., Duan L.-M. and Monroe C., *Nature*, **428** (2004) 153.
[26] Hong C. K., Ou Z. Y. and Mandel L., *Phys. Rev. Lett.*, **59** (1987) 2044.
[27] Schleich W. P., *Quantum Optics in Phase Space* (Wiley-VCH) 2005.
[28] Almendros M., Huwer J., Piro N., Rohde F., Schuck C., Hennrich M., Dubin F. and Eschner J., *Phys. Rev. Lett.*, **103** (2009) 213601.
[29] Kurz C., Huwer J., Schug M., Müller P. and Eschner J., *New J. Phys.*, **15** (2013) 055005.
[30] Schug M., Huwer J., Kurz C., Müller P. and Eschner J., *Phys. Rev. Lett.*, **110** (2013) 213603.
[31] Hulet R. G., Wineland D. J., Bergquist J. C. and Itano W. M., *Phys. Rev. A*, **37** (1988) 4544.
[32] Lindlein N., Maiwald R., Konermann H., Sondermann M., Peschel U. and Leuchs G., *Laser Physics*, **17** (2007) 927.
[33] Quabis S., Dorn R., Eberler M., Glöckl O. and Leuchs G., *Opt. Commun.*, **179** (2000) 1.
[34] Sondermann M., Maiwald R., Konermann H., Lindlein N., Peschel U. and Leuchs G., *Appl. Phys. B*, **89** (2007) 489.
[35] Stobínska M., Alber G. and Leuchs G., *Euro. Phys. Lett.*, **86** (2009) 14007.
[36] Streed E. W., Norton B. G., Jechow A., Weinhold T. J. and Kielpinski D., *Phys. Rev. Lett.*, **106** (2011) 010502.
[37] Specht H. P., Nölleke C., Reiserer A., Uphoff M., Figueroa E., Ritter S. and Rempe G., *Nature*, **473** (2011) 190.
[38] Huwer J., Ghosh J., Piro N., Schug M., Dubin F. and Eschner J., *New J. Phys.*, **15** (2013) 025033.
[39] Kurz C., Schug M., Eich P., Huwer J., Müller P. and Eschner J., *arXiv:1312.5995*, (2013) .
[40] Müller P. and Eschner J., *Appl. Phys. B*, **114** (2014) 303.
[41] Sangouard N., Bancal J.-D., Müller P., Ghosh J. and Eschner J., *New J. Phys.*, **15** (2013) 085004.
[42] Volz J., Weber M., Schlenk D., Rosenfeld W., Vrana J., Saucke K., Kurtsiefer C. and Weinfurter H., *Phys. Rev. Lett.*, **96** (2006) 030404.
[43] Stute A., Casabone B., Schindler P., Monz T., Schmidt P. O., Brandstätter B., Northup T. E. and Blatt R., *Nature*, **485** (2012) 482.
[44] Wilk T., Webster S. C., Kuhn A. and Rempe G., *Science*, **317** (2007) 488.
[45] Schubert M., Siemers I., Blatt R., Neuhauser W. and Toschek P. E., *Phys. Rev. Lett.*, **68** (1992) 3016.
[46] Moehring D. L., Maunz P., Olmschenk S., Younge K. C. and Matsukevich D. N., *Nature*, **449** (2007) 68.
[47] Slodička L., Hétet G., Röck N., Schindler P., Hennrich M. and Blatt R., *Phys. Rev. Lett.*, **110** (2013) 083603.
[48] Olmschenk S., Matsukevich D. N., Maunz P., Hayes D., Duan L.-M. and Monroe C., *Science*, **323** (2009) 486.

[49] Rauschenbeutel A., Nogues G., Osnaghi S., Bertet P., Brune M., Raimond J.-M. and Haroche S., *Science*, **288** (2000) 2024.
[50] Keller M., Lange B., Hayasaka K., Lange W. and Walther H., *Nature*, **431** (2004) 1075.
[51] Brendel J., Gisin N., Tittel W. and Zbinden H., *Phys. Rev. Lett.*, **82** (1999) 2594.
[52] Maunz P., Moehring D. L., Olmschenk S., Younge K. C., Matsukevich D. N. and Monroe C., *Nat. Phys.*, **3** (2007) 538.
[53] Stute A., Casabone B., Brandstätter B., Habicher D., Barros H. G., Schmidt P. O., Northup T. E. and Blatt R., *Appl. Phys. B*, **107** (2012) 1145.
[54] Steiner M., Meyer H. M., Deutsch C., Reichel J. and Köhl M., *Phys. Rev. Lett.*, **110** (2013) 043003.
[55] Maiwald R., Golla A., Fischer M., Bader M., Heugel S., Chalopin B., Sondermann M. and Leuchs G., *Phys. Rev. A*, **86** (2012) 043431.
[56] `http://www.uni-saarland.de/lehrstuhl/eschner`.
[57] Haase A., Piro N., Eschner J. and Mitchell M. W., *Opt. Lett.*, **34** (2009) 55.
[58] Piro N., Haase A., Mitchell M. W. and Eschner J., *J. Phys. B: At. Mol. Opt. Phys.*, **42** (2009) 114002.
[59] Schuck C., Rohde F., Piro N., Almendros M., Huwer J., Mitchell M. W., Hennrich M., Haase A., Dubin F. and Eschner J., *Phys. Rev. A*, **81** (2010) 011802(R).
[60] Piro N., Rohde F., Schuck C., Almendros M., Huwer J., Ghosh J., Haase A., Hennrich M., Dubin F. and Eschner J., *Nat. Phys.*, **7** (2011) 17.